AIP | Review of Scientific Instruments

Contributed Review: Absolute spectral radiance calibration of fiber-optic shock-temperature pyrometers using a coiled-coil irradiance standard lamp

O. V. Fat'yanov and P. D. Asimow

Citation: Review of Scientific Instruments **86**, 101502 (2015); doi: 10.1063/1.4932578

View online: http://dx.doi.org/10.1063/1.4932578

View Table of Contents: http://scitation.aip.org/content/aip/journal/rsi/86/10?ver=pdfcov

Published by the AIP Publishing

Contributed Review: Absolute spectral radiance calibration of fiber-optic shock-temperature pyrometers using a coiled-coil irradiance standard lamp

O. V. Fat'yanov[a] and P. D. Asimow[b]
Division of Geological and Planetary Sciences 252-21, California Institute of Technology, Pasadena, California 91125, USA

(Received 23 January 2015; accepted 16 September 2015; published online 19 October 2015)

We describe an accurate and precise calibration procedure for multichannel optical pyrometers such as the 6-channel, 3-ns temporal resolution instrument used in the Caltech experimental geophysics laboratory. We begin with a review of calibration sources for shock temperatures in the 3000-30 000 K range. High-power, coiled tungsten halogen standards of spectral irradiance appear to be the only practical alternative to NIST-traceable tungsten ribbon lamps, which are no longer available with large enough calibrated area. However, non-uniform radiance complicates the use of such coiled lamps for reliable and reproducible calibration of pyrometers that employ imaging or relay optics. Careful analysis of documented methods of shock pyrometer calibration to coiled irradiance standard lamps shows that only one technique, not directly applicable in our case, is free of major radiometric errors. We provide a detailed description of the modified Caltech pyrometer instrument and a procedure for its absolute spectral radiance calibration, accurate to ±5%. We employ a designated central area of a 0.7× demagnified image of a coiled-coil tungsten halogen lamp filament, cross-calibrated against a NIST-traceable tungsten ribbon lamp. We give the results of the cross-calibration along with descriptions of the optical arrangement, data acquisition, and processing. We describe a procedure to characterize the difference between the static and dynamic response of amplified photodetectors, allowing time-dependent photodiode correction factors for spectral radiance histories from shock experiments. We validate correct operation of the modified Caltech pyrometer with actual shock temperature experiments on single-crystal NaCl and MgO and obtain very good agreement with the literature data for these substances. We conclude with a summary of the most essential requirements for error-free calibration of a fiber-optic shock-temperature pyrometer using a high-power coiled tungsten halogen irradiance standard lamp. © *2015 AIP Publishing LLC.* [http://dx.doi.org/10.1063/1.4932578]

I. INTRODUCTION

Measuring the temperature of materials behind shock or detonation waves provides important constraints for defining thermodynamically complete equations of state and for understanding energy partitioning in dynamically compressed media.[1–5] Time-resolved, discrete multi-wavelength radiation pyrometry has been for several decades the most robust, reliable, and widely used tool for these studies.[6–14] As with most other spectroradiometric techniques, shock temperature pyrometry requires standard sources of light[16–19] to determine calibration factors for each pyrometer channel. Such factors are necessary to convert recorded radiance histories into equilibrium thermodynamic temperature of the material in the shock-compressed state. This is true whether the ultimate method of determining temperature is from absolute intensity[6,7,20,21] or from fitting the shape of the observed spectrum.[22,23]

The accuracy and precision of pyrometry measurements never exceeds the quality of the calibration light source. Uncertainty in its temperature or emitted light intensity will be directly inherited by the radiance or irradiance ratios and contribute to the final data uncertainty. Other potential errors in pyrometric temperature measurements are minimized when the position, size, shape, temperature range and distribution, light emission spectrum, and, in case of transient shock temperature experiments, duration of the light pulse from the calibration source and the flash from the dynamically compressed target match as closely as practically possible. Hence, shock temperature pyrometry requires highly reproducible, bright, and hot sources of broad-band, incoherent unpolarized light with accurately known absolute intensity.

Typical inert samples shock-compressed into the megabar pressure range exhibit, depending on the material compressibility, temperatures of 3000-30 000 K[1,5,6,10,20] and emissivities in excess of 0.9 in the visible spectral range.[1,24–26] Ideally, accurate calibration of fast time-response optical pyrometers would use isothermal blackbodies at the temperature range of interest. In practice, though, most reported shock temperatures above ~3000 K used pyrometers calibrated to incandescent tungsten lamps. The vast majority of these measurements employed currently discontinued tungsten ribbon standards of spectral radiance.[3,11,14,20,27,28] Less frequently, since 1983,[32,33] coiled tungsten halogen standards of spectral irradiance[5,9,10,29–31] have been used. There are only a few known exceptions to tungsten lamps for calibrating shock pyrometers.[1,4,6,23,26,34–36]

The difference between radiance and irradiance is clearly explained, for example, in Ref. 37, Ref. 38, pp. 53-58, or Ref. 15, pp. 35-37. Radiance is radiation power per unit

[a]fatyan1@gps.caltech.edu
[b]asimow@gps.caltech.edu

solid-angle-in-the-direction-of-a-ray per unit projected-area-perpendicular-to-the-ray. Irradiance is radiation power per unit area incident on the surface, from a complete hemisphere or from a particular solid angle less than a hemisphere. Spectral radiance and spectral irradiance are, respectively, radiance and irradiance per unit wavelength or frequency.

Around 2008, we started a series of radiative shock temperature measurements on preheated MgO[30] using the custom-made, 6-channel pyrometer built in our laboratory in 1994.[39,40] Using the original instrument design and calibration procedure, the data from the first two exploratory experiments showed high systematic errors in observed temperatures. Auxiliary post-shot radiometric tests revealed that optical power delivered to the photodetectors from the calibration light source was ~2.5 times lower than expected, whereas no reduction of transmitted optical power was observed for a smaller light source that simulated the actual shock target. This systematic difference in pyrometer calibration factors caused the measured shock data to be systematically higher than the actual shock temperature, by up to 1500 K at about ~6000 K.

That finding triggered two main questions: (1) are coiled-filament irradiance standard lamps a good enough alternative to largely unavailable NIST-traceable ribbon lamps for fast, high-temperature pyrometry applications? And (2), if the coiled lamp is used for shock pyrometer calibration, what conditions must be satisfied to ensure that temperature measurements are free of major radiometric errors? The main purpose of this paper is to provide clear and detailed answers to these questions. The validity of our analysis and conclusions was demonstrated experimentally and allows us to describe a laboratory procedure for ±5% accuracy in absolute spectral radiance calibration of the 6-channel, combined open-beam and fiber-coupled pyrometer in a new configuration for shock temperature measurements above ~3000 K.

II. REVIEW OF CALIBRATION SOURCES FOR SHOCK TEMPERATURE PYROMETERS

A. Low temperature range, below ca. 3000 K

The majority of the requirements mentioned above for matching the properties of calibration light sources and shock pyrometry experiments can be easily satisfied when the measured temperatures do not exceed approximately 2300 K. Many commercially available, compact blackbody simulators operate below 1800 K.[12,13,41] Some experimental models were reported that operate up to 3300 K.[42–44] However, reasonably stable and well-characterized blackbodies operating above 3000 K are quite bulky and require water cooling and inert gas purging of window-covered hot cavities.[45,46] We found only two vendors of commercial blackbody simulators operating above 2300 K.[47,48] Each of these devices weighs approximately 182 kg and has a volume of 0.7-0.8 m^3.

B. High temperature range, above ca. 3000 K

For shock temperatures above 3000 K, pyrometer calibration remains a major challenge. Table I summarizes the properties of available sources for high temperature calibration. None of the listed sources meets all requirements that we consider necessary for accurate calibration, as we review in the following paragraphs.

1. Sun

Calibration using direct imaging of the Sun is complicated by its small (~0.5°) angular size, variable atmospheric light transmittance, and changing position. Effectively infinite source distance requires either light-collecting solid angle correction for pyrometry data analysis or use instead of a live optical image of the Sun at the target position for calibration.[6]

2. Pulsed laboratory sources

Calibration by self-emission of **detonated nitromethane**[4] or **shocked quartz**[26,34] requires either two separate experiments or two pyrometers for each unknown shock temperature data point. Use of high explosive emission as a reference requires special care to prevent super-compressed detonation with significant deviation from the equilibrium Chapman-Jouguet pressure. The reference light intensity from dynamically compressed substances is never accurately known. The visible to near IR light emission spectrum from the detonation

TABLE I. Properties of light sources used for calibrating high-temperature shock pyrometers. For continuous sources, column 7 lists the exposure times of photosensors or duration of streak records in corresponding experiments. For pulsed sources, it shows full rise times or total duration of observed steady shocks.

Source	Lateral size (m)	Spatial uniformity	Temperature (K)	Emissivity	Light output uncertainty (%)	Calibration light pulse duration (s)	Measured shock temperature (K)
Sun	~0.5° linear angle	+	~5500	~1	±3	10^{-10}–10^{-7}	8000–35 000[6]
Detonating nitromethane	10^{-2}–10^{-1}	+	3700 ± 150	~1	±20	$2\cdot10^{-7}$–10^{-6}	1500–5000[2,4,22,50]
Xenon flash lamp	10^{-4}–10^{-2}	+	6000–39 000	~1	±5 to ±25	10^{-7}–$2\cdot10^{-4}$	2000–90 000[7,36,51,52]
Tungsten ribbon lamp	$6\cdot10^{-4}$ – 10^{-2}	+	2380–2800	0.41-0.47	±1 to ±3	$5\cdot10^{-5}$–10^{1}	2500–51 000[3,20,49,53]
Tungsten coiled lamp	10^{-3}–10^{-2}	–	3000–3200	0.41-0.47	±1 to ±3 irradiance, ±3 to ±5 radiance	10^{-4}–10^{1}	2500–10 800[9,30,54]
Xenon arc lamp	10^{-4}–10^{-3}	–	3500–6000	~1	±32	$3.6\cdot10^{-7}$	~14 000[35]
Shock wave in quartz	10^{-4}–10^{-2}	+	5000–50 000	~0.6-1	±20 to ±40	10^{-8}–$3\cdot10^{-8}$	5000–60 000[25,26,34]

front of pure nitromethane closely matches that of a blackbody at 3700 ± 150 K,[22] corresponding to relative uncertainty of about ±20% for absolute light intensity in that spectral range.

The relative uncertainty of reference light intensity from shocked quartz, given reported ±7%-8% relative error for shock temperature at 5000 K,[25] is about ±35% to ±40%. This uncertainty slightly decreases to about ±30% towards the highest studied quartz temperature, ~50 000 K. Similar uncertainties were reported for 5500-51 000 K shock temperatures in liquid deuterium.[49] The authors of Ref. 34 reported that in the 1-6 Mbar pressure range with a streaked pyrometer, temperatures relative to quartz emission were ~1.3× larger for polystyrene (CH) and ~1.1× larger for polypropylene (CH_2) than those based on absolute radiance measurements.[34] The advantage of shock flash light sources for shock pyrometry, partly offsetting poor precision in absolute intensity, is good match of light pulse duration between calibration and unknown shock temperature measurement.

The first application of **xenon flash lamp** as a standard light source was reported by Voitenko *et al.* in 1962.[55] The authors evaluated three different lamps using two independent time-resolved techniques — streak photography and fast 2-channel optical pyrometry — and found peak light intensities reproducible to ±5% and accurate to ±10%. Cross-calibration of these flash lamps against a tungsten ribbon standard lamp yielded brightness temperatures of 6300 ± 200 K at 650 nm and 6000 ± 200 K at 470 nm wavelengths. This type of secondary standard was used later for measuring shock temperatures of solid alkali halides[7] and in high-temperature pyrometry of shock-compressed xenon up to 50 000 K and air up to 72 000 K.[36] Modern xenon flash lamps with effective brightness temperatures from 10 000 to 20 000 K have reasonably good reproducibility of the shape of their broad-band light pulses. However, the typical time scale of variable light intensity profiles, from 10^{-6} to 10^{-4} s, exceeds the duration of a typical high-temperature shock experiment by more than an order of magnitude. Between the time-scale issue and up to 5% pulse-to-pulse variation in amplitude,[56,57] these lamps are a good choice for auxiliary pyrometer evaluation, rather than primary calibration of absolute light intensity.

3. Continuous laboratory sources

DC-powered short **xenon arc lamps** with typical brightness temperatures of 4000-6000 K have more stable light output than flash lamps. However, their use for calibration of fast pyrometers is complicated by spatial nonuniformity and poorly known size of light-emitting arcs. Results of a well documented procedure for absolute intensity calibration of nanosecond-resolved, streaked fiber-coupled spectroscopy systems using a 300 W xenon arc lamp[35] indicate ±32% uncertainty for the arc radiance and ±20% accuracy of high light intensity measurements with their streak camera/CCD system.[35]

Continuous laser-driven light sources that generate temperatures up to 10 000 K in high-pressure xenon discharge became commercially available recently.[58] All open-beam EQ-99 and EQ-1500 series products of Energetiq Technology, Inc., are specified by the manufacturer as point sources. Their light emitting plasma is about 140 μm by 60 μm FWHM and spatially nonuniform (see Figure 5 of Ref. 58), with low total optical power. The only available calibration source of this type, Energetiq EQ-99CAL, is characterized for absolute spectral irradiance only, with uncertainty of 5% to 12% depending on the wavelength. This particular xenon discharge source is inferior to OL 200, a 1000 W tungsten-halogen lamp from Optronic Laboratories, Inc., at wavelengths longer than 290 nm. EQ-99CAL irradiates ~20 times less than OL 200 at 470 nm and more than 100 times less at 800 nm.

It is not clear what area of a non-uniformly bright plasma discharge was used to evaluate spectral radiance (Ref. 58, Figures 5 and 6). Point sources can be characterized by radiant emittance or irradiance only, not by radiance.[37] Despite very high values of peak spectral radiance, ca. $1–3 \cdot 10^{13}$ W/m^3, specified by the vendors for their open-beam EQ-99 and EQ-1500 series products, these sources are obviously inferior to conventional ~1000 W coiled tungsten-halogen lamps. The authors of Ref. 59 reported brightness insufficient for electronic streak camera recording over times shorter than 10^{-7} s, 100-200 kHz emission oscillations, and 5%-10% peak light output variations for EQ-99 and EQ-99FC sources, showing that laser-driven light sources are not yet suitable for calibration of high-temperature shock pyrometry.

After fairly successful use for more than half a century,[60–64] conventional **tungsten ribbon lamps**[19] calibrated against NIST standards for absolute values of spectral radiance were discontinued. The modern alternatives to these relatively cheap yet robust and reliable light sources are **standards of spectral radiance employing integrating spheres**[65,66] and high-power quartz halogen lamps or quasi-continuous-wave lasers. These devices provide superior light uniformity over large exit aperture areas, up to 100 mm in diameter. Unfortunately, the best reported light sources of this type are 50 to 100 times dimmer than directly observed hot tungsten filaments (for example, compare Figure 9 of Ref. 63 and p. 8221 of Ref. 65 or Table IV of Ref. 66). Modern **standards based on highly scattering white screens** illuminated from a distance by a bright coiled quartz halogen lamp also yield low spectral radiances, likewise insufficient for high-temperature shock pyrometry calibration.

The only standard tungsten ribbon lamp, 30A/T24/13, currently available from NIST for more than $15k, is calibrated at 35 wavelengths from 225 to 2400 nm over a 0.6 mm wide by 0.8 mm high target area.[67] Apart from high cost, such a small area characterized for absolute spectral radiance makes use of this lamp challenging for conventional shock pyrometry. The discontinued NIST-traceable spectral radiance standard,[68] still widely used by several research groups including ours, is characterized over an area 1.5 mm wide by 5.0 mm high.

After all these considerations, high-power, quartz halogen (gas filled) **tungsten coiled-coil standards of spectral irradiance**[69,70] appear to be the most practical alternative to large-calibrated-area ribbon lamps for calibration of pyrometers above about 3000 K. The high operating temperature (3200 K vs. 2800 K for tungsten ribbon lamps) and high electric power (typically 200-1000 W vs. 75-100 W) make these lamps the brightest steady large-area sources of white light available (see

Ref. 17, pp. 97-101 and Ref. 18, pp. 251-257, for example). Their apparent drawback, however, is very nonuniform radiance, both with respect to area and direction. That is why the vendors characterize these lamps for absolute spectral irradiance only. They suggest using these lamps only for direct illumination of photodetectors from a distance of 50 cm or more, with no imaging or relay optics. Nevertheless, several practical methods have been reported[5,9,10,40] for using such irradiance standards for pyrometer calibration.

III. KNOWN METHODS OF SHOCK PYROMETER CALIBRATION USING COILED STANDARDS OF SPECTRAL IRRADIANCE

Only three published references[5,9,32] document in detail their methods of calibrating a shock pyrometer to a coiled irradiance standard lamp. References 10 and 71 each use only a single sentence to outline calibration for spectral radiance using a coiled lamp as a cross-calibrated standard. Other papers on the subject only briefly mention using a coiled lamp,[29,31,40] with insufficient information to reproduce or understand the method.

A. Boslough pyrometer

The first use of a coiled lamp for shock temperature measurements, by Boslough,[9,32] describes a calibration and operation in true spectral irradiance mode of an open-beam imaging pyrometer with no optical fibers (Ref. 15, pp. 262-268) (Figure 1). The whole lamp filament was imaged onto the 1.0 cm^2 sensitive area of each photodiode, making the lamp radiant emittance equivalent to that of a point source.[9] Calibration and measurement procedures are completely justified if there is no spot-to-spot or angular variation in photodiode response over its sensitive area. This implicitly assumed condition was valid with sufficient accuracy, at least for the photodiodes used in Caltech experiments. Since the pyrometer imaging optics demagnified the image of the lamp or shock target by only 0.3×, use of very large sensitive-area photodiodes was essential in this instrument. Unfortunately, the temporal resolution of these photodiodes, 30 ns, is too high for shock experiments in the megabar pressure range that often last only ~100-200 ns in light gas gun labs and only ~10-20 ns in laser-shock experiments.

B. Holmes pyrometer

Holmes[5] described a fiber-coupled (non-imaging) pyrometer (Ref. 15, pp. 242-252 and 637-640). For calibration, the author used an approximately 1× image of the coiled lamp created by a wide solid angle, f/1 aluminized spherical mirror (Figure 2). Unfortunately, the description of the calibration procedure is missing important details. A uniformly illuminated achromatic mirror that completely covers the acceptance angle of the optical fiber is sufficient to simulate the radiometric conditions of a shock experiment only if the lamp filament image has equal radiance at each point of the fiber core area, which is never true for coiled filament lamps. Therefore, there are several additional requirements for this procedure to be correct. First, the actual image of the hot coiled lamp filament at the fiber end must be larger than the fiber core. Implicitly assumed by Holmes,[5] this is a universal requirement for calibration of a radiance mode pyrometer.[37]

The second condition comes from the spatially nonuniform radiance of the coiled lamp filament and its image. The

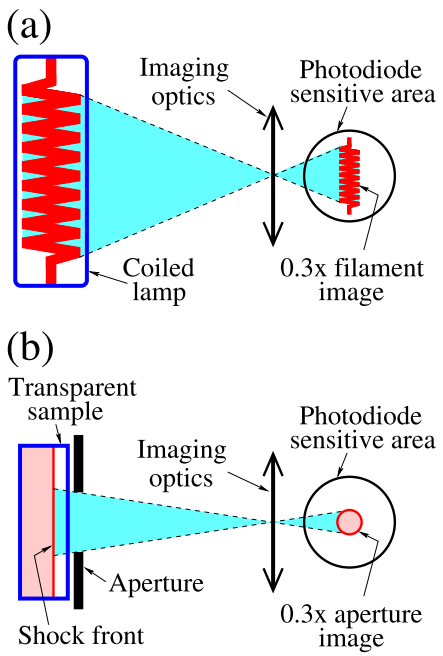

FIG. 1. Simplified schematics of Boslough pyrometer[9,32] set for the calibration (a) and shock temperature measurement (b). One channel of 4 is shown, with the photodiode rotated 90°.

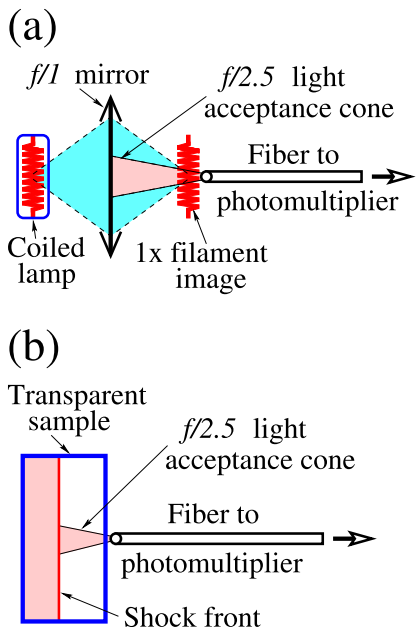

FIG. 2. Simplified schematics of Holmes pyrometer[5] set for the calibration (a) and shock temperature measurement (b). The calibration layout is drawn with refractive optics instead of the actual achromatic reflective, aluminized spherical mirror to separate the lamp from its image. One channel (multimode fiber) of 7 is shown.

fiber light transmittance function is also non-uniform, both over the core area and over the light acceptance angle. Calibration of the coiled lamp against the standard ribbon lamp will thus be valid only if the coiled filament image position on the fiber bundle remains unchanged with very high accuracy for all lamp cross-calibration and pyrometer calibration procedures. Single-stage optical averaging upon passing through individual multi-mode fibers is usually not enough to eliminate the light intensity variations due to a non-uniform source.

Holmes[5] provides no information on cross-calibrating the coiled lamp against the NIST-traceable tungsten ribbon lamp. The primary tungsten ribbon lamp standards are calibrated at NIST only over a solid angle equivalent to an f-number of 13, or a cone with a 2.2° half-angle.[67] NIST-traceable ribbon lamps from Optronic Laboratories, Inc., are characterized only over a cone with a 2.5° half-angle and are suggested to be used at no more than a 10° angle between the incident and reflected beams for the spherical mirror imaging the lamp filament.[63] These solid angles are significantly smaller than the ~11.5° half-angle acceptance cone for the fibers used by Holmes or 30° half-angle cone subtended by an f/1 spherical mirror for a point near the center of curvature. Directional emissivity curves for tungsten show measurable increases at these angles relative to the normal to the filament plane.[72] There is also apparent brightness temperature increase at angles up to 10° to the normal caused by light reflection from the glass lamp envelope, up to 13 K at 2300 K tungsten ribbon temperature.[60] If the reported cross-calibration of the coiled lamp was done with the system as described, we infer that the ribbon lamp was used well beyond the range of its NIST-traceable calibration. On the other hand, if it was done within the small solid angle specified for the ribbon lamp calibration, then we would question the validity of the coiled lamp calibration factors so determined for use with the wide-angle optics described.

C. Yang pyrometer

1. Instrument description

One more experimental approach, reported by Yang[39] and outlined by Gupta *et al.*,[40] combines the two previous methods (Figure 3). The optical layout from target to fiber bundle was a slightly modified, non-imaging version of Bosloughs pyrometer.[9,32] The second portion, from fiber bundle common end to photodetectors, was nearly identical to the stand-alone pyrometer of Holmes,[5] but with bunches of several randomized fibers instead of single fibers delivering light to each pyrometer channel. The transition from pure irradiance mode (the first pyrometer part) to pure radiance mode (the second part) was made by overfilling the acceptance angle and the entrance "pupil" of the fiber bundle with a sufficiently wide light cone from a fast relay lens (Lens #2 in Figure 3). The whole instrument was of imaging-nonimaging type, with two stages of optical averaging.[30] It was used for all shock temperature measurements in our laboratory from 1994 to 2008. An image of the coiled calibration lamp filament, demagnified by about 0.8×, was formed on the surface of a 20 mm diameter clear aperture, f/1 relay lens with its rear focal point nearly coincident with the common end face of a 6-branch fiber

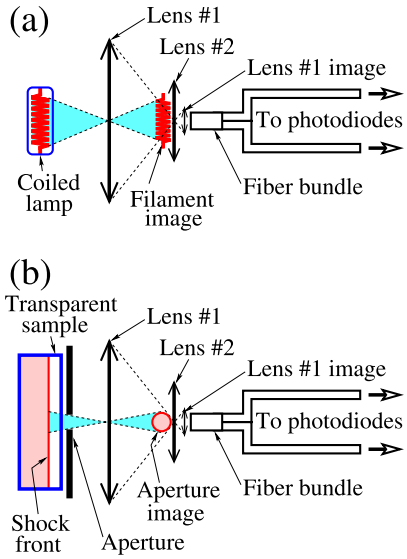

FIG. 3. Simplified schematics of Yang pyrometer[39,40] set for the calibration (a) and shock temperature measurement (b). Two channels of 6 are shown. The target aperture image is drawn rotated 90°.

bundle. The pyrometer optics up to the fiber bundle (the first part) formed a classic slide projector scheme when the almost uniformly bright area of the second imaging lens, rather than the non-uniformly bright lamp filament image, was imaged onto the fiber bundle end. This portion of the pyrometer creates the first stage of optical averaging. The second stage was implemented by using the randomized, 6-branch multiple fiber bundle.

The lamp image, small lens, and the common end of the fiber bundle at the same time formed the optical scheme of the so-called Jones or near-small-source method for calibrating a radiometer.[37] The essence of this method is that a small source of light sends the same amount of optical power to the field stop (aperture) area in the focal plane of a positive lens regardless of the position of the source within the outer regular cone with its base formed by the lens.[37] The Jones method optical scheme ensured, in the designer's opinion, transmittance of radiant power to the fiber bundle common end that is totally uniform over the whole lens area and equal for every part of the lamp filament image. That is why a significantly larger, though not accurately known, rectangular area of the lens surface (about 20 mm by 4 mm) was irradiated during calibration while only a small circle near the center, typically 3-4 mm in diameter, was irradiated during actual shock temperature measurements.

2. Calibration errors

In practice, however, the optical radiation transfer function between the lens and the fiber bundle appears to be very non-uniform. Simple tests with an incandescent lamp with a tiny (<1 mm) filament revealed a smooth but fairly rapid decrease of light power coming from the bundle branches as the lamp was moved away from the center of the lens clear aperture. Light transmittance from the central portion was 10 times higher than anywhere near the edge. Our follow-up tests examining systematically high shock temperatures on MgO

showed only about 40% of expected light power from the coiled filament image of the calibration lamp actually coming through the fiber bundle while 60% was lost in transit. This gave calibration factors 2.5 times too large and was the source of systematic errors in the temperature data.

These high radiometric errors came from a combination of the uneven light transmittance for different regions of the relay lens and the different areas of that lens irradiated during calibration and actual temperature measurements. The main reason for uneven lens transmittance was strong dependence of light power passed through the bundle on the incidence angle of incoming radiation. Optical attenuation in multimode optical fibers increases with angle between the incident beam and the longitudinal fiber axis.[73–75] This is caused by lower excitation efficiency of most waveguide modes, substantially longer optical paths, and much larger number of internal beam reflections at the core-cladding interface for light propagating at an angle to the fiber axis. For very short (several dm) fibers, this angular dependence is known to become even more pronounced due to light propagating through the cladding.[76,77] Satisfying the requirement to overfill the acceptance angle with the light cone from the relay lens inevitably caused a significant fraction of incoming radiation to enter the bundle at angles exceeding the maximum value determined by the fiber numerical aperture (NA). In this particular pyrometer, light from the lens edge enters the fiber bundle at ~30°, whereas NA of 0.2 corresponds to acceptance angle of ~11.5°.

Our analysis shows that calibration using non-uniform sources of standard irradiance for pyrometers with fiber-optic components is not as straightforward as previous workers had thought. In our opinion, the only approach that can be considered free of radiometric errors is the open-beam imaging pyrometer of Boslough.[9,32] The fiber-coupled pyrometer described by Holmes is potentially free of major errors but it is unclear to readers of Holmes[5] whether the cross-calibration procedure used in that work gave accurate and reproducible results. The approach of Yang,[39] although nominally the most sophisticated of reported methods, is unfortunately subject to very large systematic errors. We determined that substantial revision of the calibration procedure and modification of the instrument were required before using it in practical shock pyrometry applications. These revisions are documented in this report.

IV. ANALYSIS OF PRACTICAL WAYS TO IMPROVE THE ACCURACY OF CALIBRATION FOR THE EXISTING CALTECH 6-CHANNEL SHOCK PYROMETER

A. Untested modifications rejected after theoretical evaluation

Accurate pyrometer calibration to a coiled filament lamp was demonstrated for an open-beam imaging pyrometer in pure irradiance mode with large sensitive-area, slow photodetectors. However, imaging the entire ~28 mm long hot filament onto available 0.8 mm diameter fast photodiodes calls for at least 35× demagnification of the final lamp filament image. This would significantly reduce the system acceptance angle and, consequently, the efficiency of light collection from the calibration lamp or shocked target.

Changing the optical coupling to the existing fiber bundle from radiance to irradiance mode, having the large achromatic lens imaged entirely on the common end area, is not practical either. It would require at least 9× reduction of the solid angle subtended by a new relay lens while keeping the diameter of the achromatic lens image it creates below 5 mm. For the same large achromats and consequently the same size of filament image they form at the relay lens, that condition leads to a set of conflicting requirements for the pyrometer optical design. Moreover, the light transmittance function for the available bundle is not constant even within its acceptance angle limited by the fiber NA of 0.2.

Using a reduced lamp image at the target position instead of the filament itself would not completely solve the systematic error problem with Yang's original pyrometer. Even if the filament image size at the target position were to match the diameter of the limiting aperture on a shock target, the measurements would still not be completely error-free because of the non-uniform light transmittance function over the relay lens area. Removing the relay lens and imaging the whole lamp filament directly onto the fiber bundle common end area would not resolve the problem either. The bundle is assembled from close-packed cladded fibers. The polished faces of its common end and legs have only half the total optical area occupied by isolated fiber cores. The rest is covered by claddings and voids. This design is highly unfavorable for the optical transmittance uniformity required here.

The possible use of integrating spheres or other diffuse scatterers to convert spatially non-uniform radiant power into uniform radiance was immediately ruled out because of the very low efficiency of light transmittance for such optical components, about 20%-25% for the best commercial models. Integrating spheres would also smear the fronts of fast-rising optical pulses due to significantly different optical paths and degrade the time resolution of the whole system.

B. Modifications rejected after tests

We attempted imaging of the whole coiled lamp filament onto the core of a single multimode fiber that delivered full-spectrum light directly to one of the photodetectors, but this does not give reproducible enough radiometric results. The light coupling coefficient between a BFH37-400 fiber from Thorlabs, Inc. (400 μm core, 0.37 NA) and a microscope lens from Newport Corp. (20×, 0.4 NA) exhibits strong dependence on both the longitudinal distance and the lateral position of the greatly reduced filament image on the fiber core. Reproducible positioning and proper focusing of a tiny, submillimeter long, lamp filament image is a serious issue. Residual dust in the gun target chamber and uncontrolled imperfections of the polished fiber surface also have huge impacts on the accuracy of absolute light intensity measurements in this configuration. For comparison, we performed other tests using exactly the same piece of fiber overfilled by radiation from a wide-angle lens imaging the ribbon lamp filament onto the fiber core. These measurements showed fairly stable photodetector readings, reproducible to 1.5%, even at substantially

larger displacements of the flat filament image relative to the fiber tip.

The results of this analysis and exploratory radiometric experiments strongly suggested that we should implement the calibration procedure in a traditional radiance measuring configuration. We first tried to overfill the acceptance angle of the fiber bundle of the existing pyrometer with the relay lens removed with a sufficiently wide coiled filament image projected directly on the bundle end face, the way it would be done with a conventional standard of spectral radiance. However, the light power delivered to the photodetectors in this pyrometer configuration is too sensitive to the (primarily lateral) position of the filament image on the bundle end face. The spatial averaging capability of the randomized fiber bundle alone is not sufficient to filter out variations in the photodetector readings caused by small changes in the position of the lamp image and noticeable temperature nonuniformities of the hot coiled filament. This is true at least for the ~900 W, OL 200C irradiance standard calibrated for use at 8.0 A by Optronic Laboratories, Inc. (DXW 1000W 120V T5 R7s type lamp from General Electric).

Similar features were observed when a ~4× demagnified lamp filament image was projected first on an additional 2 m long patch cord of multimode fiber (1 mm core diameter, 0.39 NA from Thorlabs, Inc.) that relayed light to the whole fiber bundle via an imaging lens. There are substantial variations of transmitted light intensity depending on the longitudinal and lateral position of the filament image relative to the fiber core. These light intensity measurements were done over ~10 nm half-width discrete bandwidths from 500 to 830 nm, with the best focusing at 660 nm wavelength. Similar behavior of the optical signals recorded at different wavelengths rule out the chromatic refracting optics as a possible cause. Achromatic reflecting optics would produce a better quality image of the lamp filament but this is not practical because of the gun instrument tank dimensions and very high temperature of the operating lamp. The high heat flux makes everything within ~20 cm quite hot and could easily alter the properties of nearby reflective optics.

C. Our final approach

Both types of tests show that the averaging capabilities of the fiber bundle, whether alone or in tandem with a single multimode fiber, are not in general sufficient to get equal pyrometer readings for an arbitrary part of the coiled lamp filament used as a radiance calibration source. Therefore, we restored the original pyrometer layout with two stages of spatial optical averaging and simply chose to restrict the use of our coiled lamp to a particular central portion of its filament area. We added a 2 mm diameter field stop right on the relay lens front surface. This diameter is the optimal compromise between collected radiant power and sensitivity to transverse lamp displacements.

We also employ a 0.7× demagnified image of the lamp filament at the shock target position rather than the lamp itself. This image reduction is an important modification for several reasons. It provides a better match between the lateral size of the NIST-traceable ribbon lamp and the reduced image of the irradiance lamp filament. It better simulates the planar radiation source of a shock front by reducing the longitudinal spread of the hot filament image. Compared to the actual size of the filament, manual alignment of the reduced image onto the relay lens aperture is much simpler and allows reproducible positioning of the assigned "standard" part of filament image to within 0.05-0.1 mm. Also, such an arrangement of the calibration source significantly reduces the amount of stray light from the 900 W lamp. The lamp now sits about 0.5 m from the target position in the gun tank and does not illuminate the pyrometer optics from the side.

V. DESCRIPTION OF THE MODIFIED PYROMETER

A. Geometry and components

1. Altered first portion

The detailed optical layout of the modified pyrometer is shown in Figure 4. Optical radiation from the calibration source or the shock target is first reflected 90° by an expendable front-surface, protected-silver mirror (PF10-03-P01 from Thorlabs, Inc.) to an optical port in the target chamber covered by a 12.7 mm thick Lexan window to seal the vacuum and protect optics from debris. Wavelength-dependent optical transmittance of Lexan is not an issue since the same window is used for the calibration and the shock temperature measurement.

Two 50 cm focal length, 11 cm diameter clear aperture achromatic doublets outside the vacuum chamber form a 0.8× demagnified image of the target or calibration lamp filament on a black anodized aluminum shim with a 2 mm diameter aperture at the center. This shim makes the instrument field stop right on top of a 20 mm focal length, 20 mm clear aperture biconvex relay lens that delivers light to the common end face

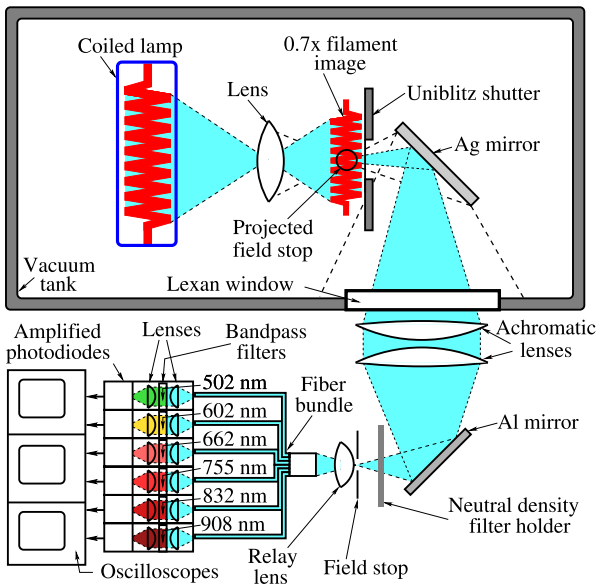

FIG. 4. Complete schematic of the modified Caltech pyrometer in calibration mode. Large achromatic lenses are shown as Lens #1 and the small relay lens is shown as Lens #2 in Figure 3. The projected circular field stop area is shown rotated 90° for clarity.

of a randomized, 6-branch custom multiple fiber bundle from Oriel Corp. It has a 10 cm long, 5 mm diameter common end and 20 cm long, 2 mm diameter legs, and consists of approximately 1200–1250 total fused silica fibers with 100 μm core size and 0.2 NA.

The original pyrometer had a well-focused light spot over ~6 mm in diameter at the bundle common end face, about 20 mm from the relay lens surface. Reducing the diameter of the relay lens clear aperture by a factor of 10 using the field stop allows us to increase optical coupling to the bundle by bringing its end closer to the lens. The size of the partially defocused light spot is smaller there and better matches the diameter of the fiber bundle end face. A good trade-off between somewhat degraded spatial light uniformity and measurably increased light coupling was found for ~10 mm distance between the lens and the bundle end face where the new light spot diameter is ~5.2 mm.

2. Unchanged second portion

The rest of the pyrometer is essentially the same as described in Refs. 39 and 40. Each fiber branch goes into an individual light-tight box attached to an amplified PIN silicon photodetector (model 1801 from New Focus, 3 ns rise time, DC-125 MHz bandwidth at 3 dB, sensitive from ~400 to 900 nm). A pair of identical plano-convex uncoated lenses with 15 mm focal length and ~11 mm diameter clear aperture inside each unit collimates and refocuses light onto the 0.8 mm^2 photodiode sensitive area. The wavelength for each unit is selected by a 10 nm FWHM bandpass filter placed between the lenses, in the region of a collimated beam. Electronic signals are recorded on Tektronix DPO4034 oscilloscopes at full 350 MHz analog frequency and 2.5 Gsamples/s. For this bandwidth, the highest noise level is 30 mV peak-to-peak. Linear response of photodetectors to the power of incoming optical radiation is observed up to at least 1.5 V output voltage.

B. Accuracy and reproducibility of calibration

This configuration was proven to be least sensitive to the coiled lamp image position and related radiance nonuniformity over the pyrometer field of view. Moving the lamp such that the filament image shifted ~0.2 mm left or right from the "standard" position (set by eye) at the field stop decreases measured light power 4% or 5% for any channel. Shifting the filament image by about 0.4-0.5 mm left or right, which is about the maximum before the rectangular perimeter of the image stops covering the circular field stop, decreases signals by 10%. Even larger vertical shifts of the lamp result in no more than ±3% deviation from the "standard" radiance value. Reproducibility of the optical signals for trials in which the lamp is removed from the tank and then put back, realigned, and refocused is typically better than 2%. This is only slightly higher than the best reproducibility level of our photodetectors, determined in a series of consecutive measurements with the lamp and detectors properly warmed up and kept continuously on, recorded by either Keithley multimeter or oscilloscopes. The relative difference in recorded voltages for such measurements was never the same for all photodetectors; it arbitrarily changes its amplitude and sign but always stayed below ±1.5% and was often within ±1.0% for both types of voltage measuring devices.

C. Size-of-source effect check

The size-of source effect is always a serious issue for imaging pyrometers focused at infinity[78] because they "see" light from any point inside the area that is equal or even slightly bigger than the clear aperture of their focusing lenses (e.g., Ref. 37, Figure 6). It could also be an issue for certain types of non-imaging pyrometers.[79] However, for imaging pyrometers with good optics set for ~1× target magnification, this effect is usually very low, 0.1%–0.2% or less (e.g., Figure 7 of Ref. 80 or Figure 2 of Ref. 81). Our instrument forms a 0.8× demagnified target image on the 2 mm diameter field stop. It is unlikely for our high quality achromatic lenses to deliver any significant amount of unwanted radiation from any point outside the 2.5 mm diameter circle on the actual target. However, we performed a test.

We removed the Uniblitz shutter and put an iris aperture at the coiled lamp filament image (see Figure 4). The iris was aligned such that its image became concentric with the field stop aperture. Then, we set the iris diameter to 4.5 mm, the size of target aperture in most shock temperature experiments calibrated as described herein, and recorded the photodiode signals with our Keithley 2000 6½-digit multimeter. After that, we opened the iris and repeated the measurements. As expected, no difference was found in the pyrometer output within the reproducibility of measurements discussed above.

VI. CHARACTERIZING THE COILED LAMP IMAGE FOR ABSOLUTE SPECTRAL RADIANCE

A. General requirements

The optical scheme of the modified instrument provides sufficient spatial optical averaging without sacrificing overall light transfer efficiency. This approach permits sufficiently accurate and highly reproducible calibration with a high-power, though non-uniformly bright, coiled-coil lamp, once the spectral radiance for the selected central portion of its filament image is determined. The advantages of characterizing and certifying tungsten lamp standards for directly measured absolute spectral radiance or irradiance rather than computing their radiative properties from the observed filament temperatures and published values of tungsten emissivity[82] are clearly explained in Ref. 16.

No calibration of a secondary or tertiary standard for absolute intensity radiometry can be achieved without reference to some primary standard. The only NIST-traceable standard of spectral radiance available to us was the tungsten ribbon lamp described in Section II B 3. Other primary sources could be used for the coiled lamp cross-calibration, such as blackbody simulators operating above ca. 2300 K. This option would greatly simplify the whole procedure because a reference source with large enough calibrated radiating area would eliminate the need for half-area calibrations described below.

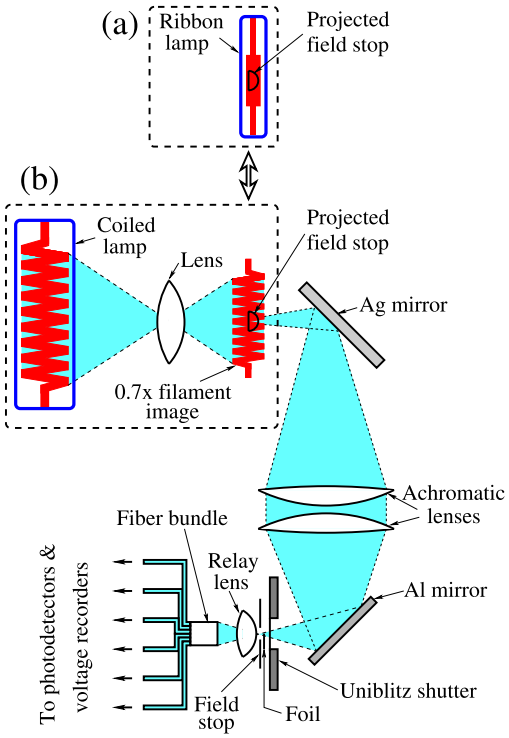

FIG. 5. Schematic of the coiled lamp image cross-calibration for half the target area: (a) ribbon lamp reference measurements followed by (b) coiled lamp radiance measurements. The projected field stop area (half-circular) is shown rotated 90° for clarity.

B. Justification of our procedure

The "standard" portion of the coiled lamp image was cross-calibrated against the NIST-traceable tungsten ribbon lamp using our 6-channel pyrometer (Figure 5). The same geometry, optical layout, and wavelength filters were used as in actual shock-temperature experiments, with two minor exceptions: the Lexan window was removed to increase signal levels and only half of the coiled filament target area was characterized at a time. Such a two-step calibration procedure was necessary because the ~2.5 mm diameter "standard" circle on the 0.7× demagnified image of the coiled filament exceeded the 1.5 mm wide working area of the primary ribbon lamp filament. Light was collected over a cone with a half-angle of 6°, which is more than the 2.5° where the ±2%-3% accuracy of ribbon lamp calibration is guaranteed. However, possible variations of radiance due to reflection from the glass lamp envelope are more than two times smaller at angles from the normal to the filament plane between 2.5° and 6° than they are between 0° and 2.5°.[60] The directional emissivity of polished tungsten for these angles is indistinguishable from the values normal to the filament plane.[72] This ensures that the radiative properties of the primary lamp filament and of planar shock front both obey the same Lambertian-type cosine law, which, in turn, justifies the validity of our calibration.

C. Cross-calibration # 1

The first cross-calibration was done with a 50 mm diameter, 75 mm focal length double-convex, uncoated glass lens that formed an ~0.7× demagnified image of the coiled filament at the shock target position. Photodetector output voltages were measured on the 6½-digit multimeter with a maximum ±0.04% relative uncertainty. To account for background drift of the amplifiers, the average of two "dark" signal measurements taken before and after was subtracted from each "light" measurement.

In practice, we first blocked half the field stop area with thin copper foil. The ribbon lamp was aligned and focused on the half-circle with its diameter oriented along the filament image and the lamp position marked on an optical rail. After the first series of measurements with the ribbon and then the coiled lamp, we blocked the other half of the field stop area and took the second series of data from the coiled lamp that was still running. Finally, the ribbon lamp was reinstalled at its marked position and translated to overfill the new open half-circle in the field stop for the last series of measurements. As instructed by Optronic Laboratories, Inc., each lamp was warmed up for 20 min prior to use. This cross-calibration procedure involves manually estimating the orientation of the half-circle diameter, but our results indicated negligible sensitivity to this orientation.

Table II shows fairly good agreement between data from the two halves of the coiled lamp image (columns 2 and 3). The average values of cross-calibration factors at 6 wavelengths and their relative precisions are listed in columns 4 and 5. Column 6 lists the measured spectral radiance for the portion of the coiled filament we calibrated. For comparison, column 7 shows the recalculated average spectral radiance for the whole filament from the spectral irradiance calibration

TABLE II. Summary of the first cross-calibration of a 0.7× coiled-coil lamp filament image for absolute spectral radiance (thin uncoated glass lens, Keithley 2000 multimeter). All values have one additional insignificant digit included to increase the resolution.

	Cross-calibration factors				Absolute spectral radiance, W/m^3			
Wavelength (nm)	Half-circle #1 data, R_1	Half-circle #2 data, R_2	Average of R_1 and R_2	Relative precision of measurements (%)	Measured against ribbon lamp, N_1	Calculated from irradiance data, N_2	Ratio of measured to calculated, $m = N_1/N_2$	Normalized by average ratio, $k = m/\bar{m}$
502.0	6.432	6.869	6.650	3.3	1.893×10^{11}	1.741×10^{11}	1.087	1.005
602.0	5.093	5.343	5.218	2.4	3.556×10^{11}	3.249×10^{11}	1.095	1.011
662.0	4.506	4.828	4.667	3.4	4.404×10^{11}	4.028×10^{11}	1.093	1.010
755.0	3.892	4.184	4.038	3.6	5.231×10^{11}	4.893×10^{11}	1.069	0.988
832.0	3.644	3.816	3.730	2.3	5.637×10^{11}	5.254×10^{11}	1.073	0.991
909.0	3.454	3.583	3.519	1.8	5.770×10^{11}	5.363×10^{11}	1.076	0.994

table, assuming a radiating area of the coiled filament given by a rectangle of 25 by 5 mm (the coiled filament length and larger diameter, respectively). This approach does not account for non-radiating void areas or non-uniform radiance of different filament regions. The ratio of measured and recalculated spectral radiances and the same parameter normalized by the average value at 6 wavelengths are in columns 8 and 9, respectively. The fairly constant value of either of these parameters is a good cross-check for consistency of our measurements. The error analysis indicates ±5% maximum uncertainty of absolute spectral radiance for the coiled lamp image, due to: ±3% uncertainty for the NIST-traceable tungsten ribbon lamp, maximum 3.6% difference between two independent cross-calibration factor measurements, ±1 to ±1.5% uncertainty of our 6-channel pyrometer readings, and ±1.5% accuracy of voltage measurements on Tektronix oscilloscopes used later.

D. Cross-calibration # 2

After 50 h of operation, when recalibration of the standard lamp was due, we did another calibration against the ribbon lamp. Instead of the uncoated double-convex lens, we used a 75 mm focal length, 50.8 mm diameter achromatic lens with anti-reflection coating for the visible range, about 400–700 nm (AC508-075-A from Thorlabs, Inc.). Pyrometer signals were recorded on Tektronix oscilloscopes at 2.5 Gsamples/s for each scope channel, as in actual shock experiments. Before measurement, we performed a signal path compensation[83] for all oscilloscopes to ensure the highest accuracy, ±1.5% for measurements of order millivolts at fixed vertical gain settings in the sequence of 1:2:5, e.g., 1 mV/div, 2 mV/div, and 5 mV/div. A 6.3 mm diameter aperture Uniblitz shutter mounted before the field stop triggered the oscilloscopes once its blades fully opened. For photodetector noise filtering, we internally limited the bandwidth of the oscilloscope channels to 20 MHz and computed each value as an average of all 10^5 recorded data points. Insignificant difference was found when the data were recorded at full oscilloscope bandwidth of 350 MHz or using 10^6 points.

Two "light" signals for each channel were bracketed by three "dark" background measurements. As the precision of background-subtracted signal measurements in the same series was much better than uncertainties from other known error sources, these redundant data were used for internal consistency checking only.

The summary of our second cross-calibration is shown in Table III. Most values are higher than the first cross-calibration (compare column 4 of Tables III and II), due to the 400 to 700 nm broad-band anti-reflective (AR) coating of the achromatic lens. As seen in column 8, the relative radiance of the filament image was significantly lower for the 437 nm channel and measurably lower for the 755 nm channel compared to the other 4. The shortest filter wavelength, 437 nm, is in the high absorption band at wavelengths shorter than ~500 nm in E-BAF11 (barium flint) and N-SF11 (dense flint) lens glass. The longest filter wavelength, 755 nm, is outside the peak transmittance window of the AR-coating. No simple comparison between the values of spectral radiance measured relative to the ribbon lamp and recalculated from the spectral irradiance calibration data could be done at these wavelengths. These ratios are included in column 8 of Table III for completeness but are excluded from calculation of the average ratio $\bar{m}$ used for computing column 9.

VII. CHARACTERIZING THE DIFFERENCE BETWEEN DYNAMIC AND STATIC RESPONSE OF PHOTODETECTORS

The shortest light pulses formed by our Uniblitz shutter have full rise time of ~500 μs before reaching a flat-top plateau where the actual calibration data are taken. This exposure time for the photodiodes is more than 3 orders of magnitude longer than the total duration of our shock temperature measurements.

A. Measurements at 660 nm

We examined the transient response of our photodetectors to fast-rising optical pulses of nearly constant amplitude using the BNC model 6010 light pulse generator from Berkeley Nucleonics Corp. (10 ns rise time, 660 nm, 50 μW maximum power). For the same optical input, an electronic signal from each photodetector was compared to a direct output from a fast Valyn International photomultiplier (1 ns rise time RCA-7764 tube with S-11 photocathode sensitive from 300 to 660 nm). The vendor provided a special electronic circuit similar to the one described by Beck[84] for improved time response of the

TABLE III. Summary of the second cross-calibration of a 0.7× coiled-coil lamp filament image for absolute spectral radiance (thick AR-coated achromatic lens, Tektronix DPO4034 oscilloscopes). All values have one additional insignificant digit included to increase the resolution.

	Cross-calibration factors				Absolute spectral radiance, W/m^3			
Wavelength (nm)	Half-circle #1 data, R_1	Half-circle #2 data, R_2	Average of R_1 and R_2	Relative precision of measurements (%)	Measured against ribbon lamp, N_1	Calculated from irradiance data, N_2	Ratio of measured to calculated, $m = N_1/N_2$	Normalized by average ratio, $k = m/\bar{m}$
437.0	6.874	6.807	6.841	0.5	7.807×10^{10}	8.817×10^{10}	0.886	
502.0	7.664	7.283	7.474	2.6	2.127×10^{11}	1.741×10^{11}	1.222	1.002
553.0	6.545	6.562	6.554	0.1	3.121×10^{11}	2.509×10^{11}	1.244	1.020
602.0	5.805	5.825	5.815	0.2	3.963×10^{11}	3.249×10^{11}	1.220	1.000
662.0	5.081	5.093	5.087	0.1	4.800×10^{11}	4.028×10^{11}	1.192	0.977
755.0	4.417	4.428	4.422	0.1	5.730×10^{11}	4.893×10^{11}	1.171	

tube. The maximum noise level at full recording bandwidth (350 MHz analog, 1.25 or 2.5 Gsamples/s digital) was about 5 mV and the vendor-specified linearity range was up to 25 mV output voltage into a 50 Ω load.

The ability of photodetectors and the photomultiplier to reproduce constant intensity light pulses was first tested using the coiled standard lamp in a typical pyrometer calibration arrangement. The results indicated constant output level for all amplified semiconductor photodiodes but linearly increasing signal from the photomultiplier at ~0.25% per 100 μs for the flat-top light pulse plateau (Figure 6). The brightening rate of the photomultiplier was nearly independent of light pulse duration and amplitude. This feature of the photomultiplier was taken into account when the photodiode response to shorter, fast-rising optical pulses was analyzed.

The high stability and reproducibility of the BNC generator optical output allowed us to improve the signal-to-noise ratio of recorded analog voltages by internal averaging of 512 consecutive pulses on Tektronix oscilloscopes. By comparison with direct unamplified output from the photomultiplier, it was found that all New Focus amplified photodiodes respond to light pulses that are best approximated by the Heaviside step function with a 14%–19% increase in electronic output amplitude over ~50 μs period. At later times, no detectable change of output voltage was found.

On the falling edge of the light pulse, the electrical output signals of the photodiodes never go directly back to zero. They first fall to some positive value that later relaxes back to zero with about the same ~50 μs time constant on every detector tested. No effort was made to quantify possible corrections to the photodiode response functions after fast optical power decrease because of the enormous variety of potential shapes and amplitudes of light pulses from real shock targets.

The choice of the Valyn International photomultiplier as a reference detector, with due regard to its spurious slow ramping, was confirmed later using the fast photodetector from LLNL pyrometer[5,84] (ultra-low-noise Hamamatsu R928 tube with multialkali photocathode sensitive from 185 to 900 nm). The shape of its output electronic signal was virtually identical to that from the Valyn International photomultiplier, at least for

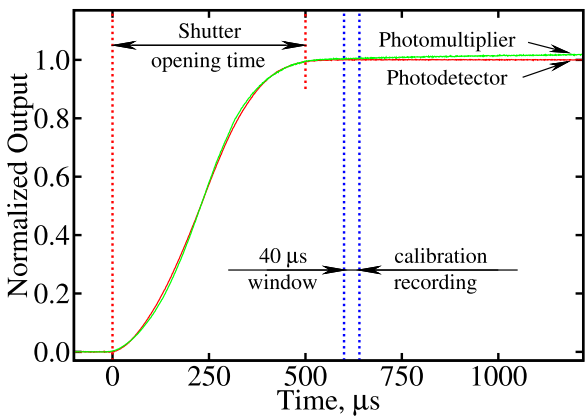

FIG. 6. Typical normalized output signals from the standard lamp recorded with Valyn International photomultiplier and New Focus amplified semiconductor detector. About 500 μs rise time is the shortest attainable by Uniblitz shutter in our optical configuration. Data acquisition for the actual pyrometer calibration starts about 100 μs after the shutter fully opens.

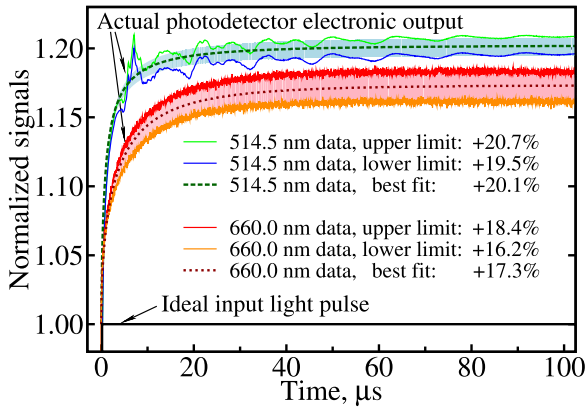

FIG. 7. Normalized electronic output response of our 1801 New Focus amplified semiconductor detectors to Heaviside step input light function measured at 514.5 and 660.0 nm. All bandpass filters were removed for these tests. The upper and lower limit data curves and the shaded areas between the corresponding best fits indicate the precision of our measurements. All reference light pulses were recorded with the same LLNL photomultiplier. Reproducible irregularities on 514.5 nm experimental results are artifacts of the Pockels cell operation.

up to 500 μs long, nearly flat-topped, 10 ns rise-time optical pulses. The only difference was the absence of any detectable ramping of the LLNL photomultiplier output comparable to the artifact in the Valyn International photomultiplier output. In all subsequent measurements of the photodiode dynamic response, the LLNL photomultiplier was the primary "standard" detector.

More tests with the BNC 6010 light pulse source at maximum optical power that generated ~50–100 mV voltage yielded 16.2%–18.4% increase of electronic output amplitude (Figure 7). The upper and lower limit values are quite reproducible but not necessarily exhibited by the same photodetectors. Within the total estimated uncertainty of ±2%, the transient response curves of all our New Focus detectors are the same.

B. Measurements at 514.5 nm

The BNC 6010 pulsed light source available to us was not bright enough to generate more than ~100 mV output voltage for the amplified photodiodes. Typical voltage pulses recorded in our shock experiments are 300–700 mV. The photodiode output "ramping" at these levels of input optical power was examined using a 514.5 nm Ar ion laser (Lexel laser, Inc., Model 95) and a Pockels cell (Q/X 1630 from Cleveland Crystals, Inc., powered by Lasermetrics Model 8025 high-voltage pulse generator). The Pockels cell forms a single high power laser pulse with 100 ns rise time and ~500 μs duration. This optical pulse is approximately flat-topped, with some transient features and damped oscillations up to ~100 μs.

Measurements were performed at six levels of input optical power generating approximately 100, 300, 500, 700, 900, and 1100 mV output voltage. The transient response at 514.5 nm wavelength was nearly independent of the amplitude. The individual response functions were also the same, within the total ±2% uncertainty of measurements, for all photodetectors. The average results of 4 measurements at 300, 500, 700, and 900 mV output voltage are shown in Figure 7.

TABLE IV. Summary of dynamic response correction factors for our New Focus photodetectors at two wavelengths.

	Wavelength (nm)	
Light pulse duration (μs)	514.5	660.0
0.1	1.17 ± 0.03	1.15 ± 0.03
0.2	1.15 ± 0.03	1.14 ± 0.03
0.4	1.12 ± 0.03	1.12 ± 0.03
0.8	1.09 ± 0.03	1.10 ± 0.03

Insignificant difference is observed if the data taken at 100 and 1100 mV are included.

C. Summary of all transient response results

The best fit expressions for the photodetector dynamic response at 514.5 nm and 660.0 nm wavelengths are, respectively,

$$f1(t) = 1.2024 - 0.648 \cdot (e^{-1.886\cdot(t+0.186)^{0.287}}) \quad (1)$$

and

$$f2(t) = 1.1734 - 0.174 \cdot (e^{-0.5036\cdot(t+0.0001)^{0.550}}), \quad (2)$$

where t is time in microseconds from the beginning of measured light pulse. Both functions fit their data sets quite well and satisfy the initial condition of $f1(t = 0) = f2(t = 0) = 1$. Equations (1) and (2) were used to compute the light intensity correction factors for the typical duration of our shock temperature experiments (Table IV). Despite some obvious discrepancy in amplitudes and shapes of the dynamic response functions at 514.5 and 660.0 nm (see Figure 7), the corresponding correction factors at all times of interest are nearly the same.

We do not know whether the actual photodiode output "ramping" at constant input light power will be the same at wavelengths longer than 660 nm. Normalized time-dependent radiance histories from ~700 ns long shock temperature experiments in NaCl are indistinguishable for all wavelengths from 602 to 832 nm. This fact may suggest very similar transient response of our New Focus photodetectors over this particular spectral range. For comparison, Ref. 85 reports secondary response distortion — which is simply another name for the photodiode transient response — as an essentially wavelength-dependent function at wavelengths above 900 nm for FND100Q and at wavelengths below 1000 nm for GAP520 photodiodes. However, the substantial differences between the static and dynamic responses of the New Focus amplified photodetectors reported here provide at least partial explanation for the ubiquitous ramping of radiance histories from shocked samples observed in our laboratory.

VIII. VALIDATION OF OUR CALIBRATION PROCEDURE

A. NaCl test at 7500 K

The new calibration procedure using a coiled lamp as a standard of spectral radiance was first checked in a test shot on single-crystal sodium chloride. Both optical and thermodynamic properties of this substance in shock-compressed states have been extensively studied by several research groups and are considered well known. Raw radiance histories for this shot are shown in Figure 8. As in Lyzenga's experiments,[8,86] we observed fast, ~10 ns, rise time of optical signals, followed by noticeable ramps. Similar apparent gradual brightening of steady radiative shock fronts was also observed, for example, in fused quartz (Ref. 3, Figure 5), cesium iodide (Ref. 54, Figure 1), and calcite (Ref. 40, Figure 3).

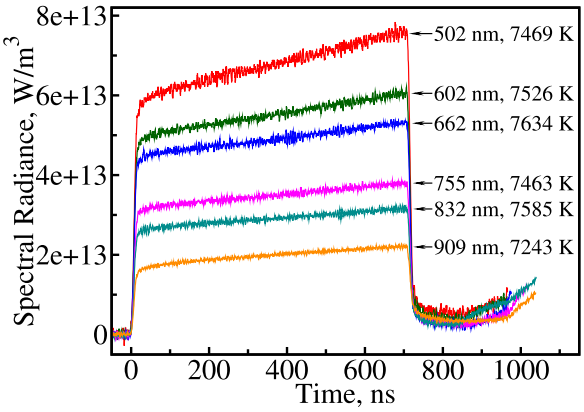

FIG. 8. Absolute spectral radiance histories and corresponding shock temperatures observed in ⟨100⟩ NaCl crystal shock compressed to 102 ± 2 GPa.

The most obvious and experimentally confirmed reason for that phenomenon is transient response of semiconductor photodetectors discussed above. Another untested effect is increasing apparent shock front emissivity as it approaches the sample free surface. Since the unshocked crystal, although transparent, has a refractive index greater than 1, there is always some fraction of light returning back to the radiating shock front due to total internal reflection of low angle-of-incidence rays reaching the sample-vacuum interface. This fraction and the area of the planar radiating shock front that receives the back-reflected radiation both increase with time as the shock wave nears the sample free surface.

The radiative temperature data analysis of Lyzenga was done by simultaneous two-parameter nonlinear least-squares fitting for temperature and emissivity,[3,32,40,54,86] assuming equal response of the photodiodes during calibration (~10^{-2} s) and measurement (~10^{-8}–10^{-7} s).[86] Due to the much weaker dependence of spectral radiance on emissivity than on temperature, this procedure often leads to spurious emissivities (e.g., greater than unity if not bounded)[33,40] and, in such cases, incorrect temperature values. Most emissivities for shocked NaCl determined from this gray-body fitting approach[86] are in apparent disagreement with values recalculated from the refractive index measured in the shock-compressed state by a straightforward geometric technique.[1,24] The same is true of numerically extracted emissivities for CsI.[54] Therefore, we reanalyzed all Lyzenga's data points using his listed values of measured spectral radiance.[86] Shock temperatures were extracted for each channel[6,7,21,30] by solving the Planck gray-body equation with wavelength-independent emissivity of 0.927 ± 0.009 recalculated from the measured refractive

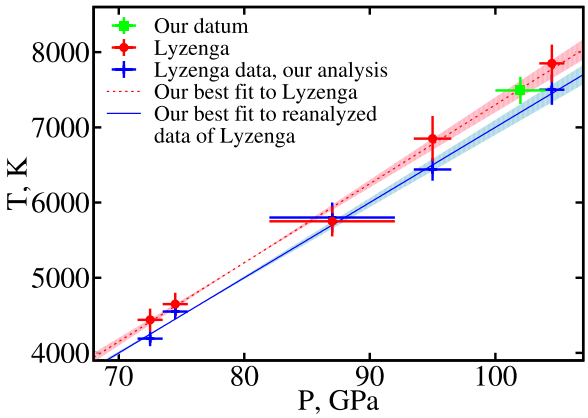

FIG. 9. Comparison of our NaCl datum with the results of Lyzenga.[86] Crosses are the actual error bars. Linear least-square fitting with errors in both coordinates was done using the method of Ref. 88. The best fits to the original Lyzenga data and the results of our analysis are, respectively, $T_0 = (-3.2 \pm 0.4) \cdot 10^3 + (105 \mp 5) \cdot P$ and $T = (-3.0 \pm 0.3) \cdot 10^3 + (100 \mp 4) \cdot P$, where T is in K and P is in GPa. The uncertainties of fits are shown as shaded areas.

indexes at ambient and shock-compressed states.[24] An average value from all wavelengths was taken for the actual shock temperature. All Lyzenga's original data and the current results including the new data point are shown in the summary plot (Figure 9). Good agreement between either set of Lyzenga data and our datum confirms the accuracy of the new calibration procedure in this experiment.

Despite reasonably good agreement between the measured shock temperatures, our new experiment and Lyzenga's experiments yield a much higher apparent optical absorption in shock-compressed NaCl, compared to the data of Kormer *et al.*[7,87] Lyzenga attributed this to the low temporal resolution of Kormer's pyrometer, but it persists in experiments with rise times from 400 to 1350 ns (Figure 5 of Ref. 7). Kormer *et al.* also observed systematically higher absorption at 478 nm than at 625 nm (e.g., Figure 1 of Ref. 87). This indicates that the different optical absorptions seen in NaCl are due to differences in sample purity and handling. NaCl crystals for Kormer's experiments were custom grown and polished by the leading Russian Optical and Mechanical Factory (currently LOMO PLC) and covered with a thin layer of transparent lacquer to protect them from moisture. The samples used in our experiments and those of Lyzenga were conventional optical windows, with no special attention paid to crystal growth, polishing, or coating procedures.

Uncoated crystals in our experiments were exposed to air for at least a few hours before the tank chamber was closed and evacuated to 0.1 Torr. This level of vacuum is insufficient to remove even surface-adsorbed water from room-temperature alkali halide crystals. For example, KBr releases the majority of adsorbed water only after heating to at least 620 K at 10^{-6} Torr.[89] Both NaCl and KCl single crystals melt-grown in wet ambient atmosphere show absorption in their "OH" bands, 185 and 204.5 nm, ~10 times higher compared to those grown in dry atmosphere.[90] Even concentrations of water in the starting NaCl undetectable by spectroscopy may significantly increase their optical absorption upon shock compression to ~1 Mbar.

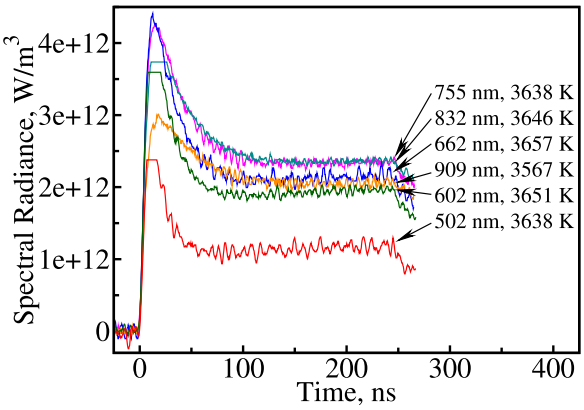

FIG. 10. Absolute spectral radiance histories and corresponding shock temperatures observed in ⟨100⟩ MgO crystal shock compressed to 195 ± 3 GPa.

B. MgO test at 3630 K

We also measured shock temperature of single-crystal MgO using the new calibration procedure. The results are shown in Figures 10 and 11. Good agreement between the values of Svendsen and Ahrens[33] and our data confirms consistency of the different calibration procedures in these two sets of experiments. Svendsen and Ahrens used the coiled spectral irradiance lamp imaged entirely onto the sensitive areas of photodiodes (Boslough configuration described above). We used a coiled lamp image that overfilled the entrance pupil and acceptance angle of the pyrometer, cross-calibrated for spectral radiance. Since the optical absorption of shocked MgO is not very high at the studied conditions, our radiance records still include some light flash from a shock-compressed layer of epoxy between the driver plate and the Ag-Cr coated impact face of MgO. Relaxation of that light pulse almost compensated the electrical signal ramps that are still visible on some pyrometer channels (Figure 10).

Our experiment yields much smaller error bars than those of Svendsen and Ahrens for several reasons: we used more pyrometer channels (6 vs. 4), we recorded better quality raw radiance signals with only a weak light flash from the sample-driver plate interface, and we introduced a more reliable

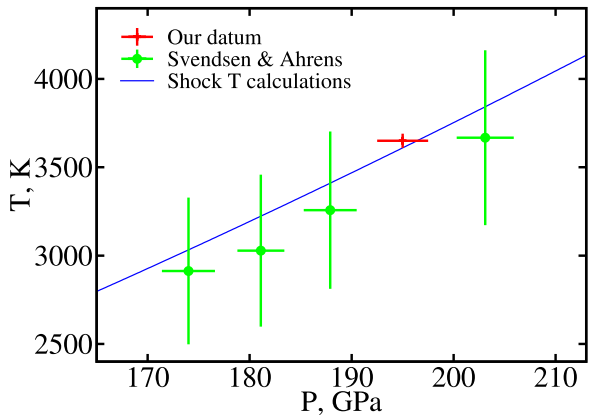

FIG. 11. Comparison of our MgO datum with the results of Svendsen and Ahrens.[33] Crosses are the actual error bars. For shock temperature calculations we used the Hugoniot reported in Ref. 91, Grüneisen values reported in Ref. 30, and Debye temperature used by the authors of Ref. 33.

procedure for shock temperature analysis. Svendsen and Ahrens used simultaneous two-parameter nonlinear least-squares fitting for temperature and emissivity, which led to unphysical emissivities in excess of 0.924 — from 1.00 to 1.19.[33] Instead, we analyzed our data as reported in Refs. 30 and 14 and described above for NaCl. The best estimated emissivity of 0.91 for our experimental conditions was computed from 7.6% Fresnel reflection at the MgO-vacuum interface and ~2% reflectivity of the shock front, evaluated using the Gladstone-Dale expression.[1]

IX. SUMMARY

A review of all reported commercial and experimental scientific calibration sources for shock pyrometry above ~3000 K confirms that high-power, coiled tungsten-halogen standards of spectral irradiance, though far from ideal for these applications, are currently the only practical choice for many reasons.

In our opinion, reproducible calibration that is free of major radiometric errors using these lamps has been clearly demonstrated only for the following two scientific pyrometers with high optical throughput schemes:

(1) Open beam (no fiber-optics) imaging instrument operating in pure irradiance measuring mode. The whole lamp filament has to be projected entirely onto large area photodiodes, which seriously limits applicability of this method to any fiber-optic coupled pyrometers or fast shock temperature measurements using small area photodetectors. This might be improved by employing fast photomultipliers and proper spatial optical averaging configuration with slide projector schemes or diffuse light scatterers. However, such an approach was not tested for the reasons mentioned in Section IV and because the dynamic range (ratio of maximum linear output voltage to the noise voltage) of Valyn International photomultipliers available to us, ~8 dB, was substantially smaller than the ~17 dB range of amplified photodetectors.
(2) Imaging-nonimaging, fiber-optic instrument operating in a traditional radiance measuring mode. Only a particular area of demagnified filament image can be used to overfill the pyrometer entrance "pupil." This designated area needs to be cross-calibrated against a NIST-traceable standard for the same optical configuration and wavelength filters as in actual shock-temperature experiments.

We were unable to demonstrate proper calibration of a pyrometer similar to one described by Holmes. We upgraded the system design by introducing a multimode fiber in tandem with the randomized bundle, to make the arrangement more robust against source radiance nonuniformity. Nevertheless, no reliable or reproducible results were obtained using a ~900 W coiled-coil quartz-halogen lamp. It is quite possible that Holmes' simplified version may demonstrate acceptable performance with some particular, more uniform lamp. However, this type of instrument was certainly found unsuitable for use with any arbitrary coiled lamp.

The modified Caltech instrument[30] described here and successful results of its use in actual shock temperature measurements provide, in our opinion, sufficient answers to both questions posed in the Introduction. The new calibration procedure was tested on two different known materials, NaCl at 7500 K (peak of radiation at 387 nm) and MgO at 3630 K (peak of radiation at 798 nm). Both experiments showed a good agreement between our shock temperature data and the values reported by other researchers that used totally different pyrometers, calibration sources and procedures, and methods of data analysis. Furthermore, we also demonstrated good agreement between the temperatures extracted for each of six individual pyrometer channels (see the values listed in Figures 8 and 10). A cancellation of hypothetical unknown errors across so broad range of measured light intensities and across two differently shaped emission spectra would be, it seems, an extraordinary coincidence.

Briefly, the most essential requirements that ensure error-free radiometric shock temperature measurements are listed below:

- Any fiber-optic pyrometer with fast, small-area photodiodes requires a traditional radiance type of calibration and measurement, with both the entrance pupil and acceptance angle of the instrument overfilled with radiation.
- The instrument has to provide adequate spatial optical averaging over its field of view with respect to both area and direction. The definition of what is "adequate" in this context strongly depends on the parameters of the coiled lamp filament and the degree of its radiance nonuniformity.
- Two stages of spatial optical averaging are not sufficient to provide accurate and reproducible calibration using an arbitrarily chosen part of a coiled lamp filament or its image, at least for the ~900 W, coiled-coil lamp we tested, which is very nonuniformly bright and has large gaps between parts of the filament. The simplest and most reliable way of addressing this issue is to employ, during cross-calibration and subsequent use, a particular part of the filament assigned as "standard."

Limited resources allowed us to perform a comprehensive study of only one particular instrument and its major modifications. Therefore, this set of requirements may not be sufficient to cover all possible scenarios.

X. CONCLUSIONS

We developed a procedure for absolute spectral radiance calibration, accurate to 5%, of a 3-ns rise-time, 6-channel combined open-beam and fiber-coupled pyrometer with 0.8 mm diameter sensitive area photodetectors. The source was a 0.7× demagnified image of a coiled-coil tungsten halogen lamp filament cross-calibrated against a NIST-traceable tungsten ribbon lamp. The image of the ~900 W coiled lamp has 3.5–7.5 times higher radiance, depending on the wavelength, than the primary ribbon lamp standard. Up to 21% differences between the static and dynamic response of New Focus 1801

amplified photodetectors were found for 514.5 nm light at optical power levels corresponding to ~300–900 mV output voltages, the same values as in actual shock temperature experiments. Similar transient response functions were measured with 660 nm light at optical power levels corresponding to ~50–100 mV voltages. The accuracy of absolute radiometric measurements reported here was validated in actual shock temperature experiments on single-crystal NaCl and MgO that spanned an input range of 18 dB.

ACKNOWLEDGMENTS

Thanks are due to the late Professor Tom Ahrens, the founder of the Lindhurst Laboratory of Experimental Geophysics at Caltech, for inviting one of us (O.V.F.) to join the research staff of this laboratory in 2006, for many interesting suggestions and advice, and for his broad interest in non-traditional methods in shock-wave physics including the topic of pyrometer calibration. Our LLNL collaborators, Dr. Neil Holmes and Dr. Jeff Nguyen, are gratefully acknowledged for their pyrometer and Pockels cell that largely extended the transient response characterization of our photodetectors. Professor George Rossman of Caltech helped with operating his visible range and FTIR spectrometers and shared his extensive knowledge about water contamination of minerals. Former technical staff members of the Lindhurst Lab Mike Long, Papo Gelle, and Russ Oliver provided expert assistance with the two-stage light-gas gun experiments. O.V.F. thanks his wife Elena who reviewed the very first draft of this manuscript and made the whole narrative substantially smoother. Valuable comments and suggestions by anonymous reviewers that helped improve the manuscript and made it more accessible are really appreciated. The financial support came from the U.S. NSF, Award No. EAR-1426526.

[1]S. B. Kormer, Sov. Phys.-Usp. **11**, 229 (1968) [Usp. Fiz. Nauk **94**, 641 (1964)].
[2]I. M. Voskoboinikov, V. M. Bogomolov, A. N. Afanasenkov, and V. N. Shevelev, Sov. Phys.-Dokl. **13**, 1026 (1968) [Dokl. Akad. Nauk SSSR **182**, 807 (1968)].
[3]G. A. Lyzenga and T. J. Ahrens, Rev. Sci. Instrum. **50**, 1421 (1979).
[4]M. F. Gogulya and I. M. Voskoboinikov, Combust., Explos., Shock Waves **24**, 759 (1988) [Fiz. Goreniya Vzryva **24**, 127 (1988)].
[5]N. C. Holmes, Rev. Sci. Instrum. **66**, 2615 (1995).
[6]I. Sh. Model', Sov. Phys. JETP **5**, 589 (1957) [J. Exptl. Theoret. Phys. (U.S.S.R.) **32**, 714 (1957)].
[7]S. B. Kormer, M. V. Sinitsyn, G. A. Kirillov, and V. D. Urlin, Sov. Phys. JETP **21**, 689 (1965) [J. Exptl. Theoret. Phys. (U.S.S.R.) **48**, 1033 (1965)].
[8]G. A. Lyzenga, AIP Conf. Proc. **78**, 268-276 (1982).
[9]M. B. Boslough and T. J. Ahrens, Rev. Sci. Instrum. **60**, 3711 (1989).
[10]H. B. Radousky and A. C. Mitchell, Rev. Sci. Instrum. **60**, 3707 (1989).
[11]A. Pyalling, V. Gryaznov, S. Kvitov, D. Nikolaev, V. Ternovoi, A. Filimonov, V. Fortov, D. Hoffmann, C. Stockl, and M. Dornik, Int. J. Thermophys. **19**, 993 (1998); V. Ya. Ternovoi, A. S. Filimonov, S. V. Kvitov, A. A. Pyalling, D. N. Nikolaev, Yu. E. Gordon, and V. E. Fortov, High Temp.-High Pressures **34**, 73 (2002).
[12]D. Partouche-Sebban, D. B. Holtkamp, P. Rodriguez, J. B. Stone, S. D. Borror, C. A. Kruschwitz, and J. A. Young, Rev. Sci. Instrum. **76**, 013106 (2005).
[13]B. M. LaLone, G. D. Stevens, W. D. Turley, D. B. Holtkamp, A. J. Iverson, R. S. Hixson, and L. R. Veeser, J. Appl. Phys. **114**, 063506 (2013).
[14]O. V. Fat'yanov and P. D. Asimow, J. Phys.: Conf. Ser. **500**, 062003 (2014).
[15]D. P. DeWitt and G. D. Nutter, *Theory and Practice of Radiation Thermometry* (Wiley, New York, 1988).
[16]W. E. Schneider and D. G. Goebel, Proc. SPIE **262**, 74 (1982).
[17]R. Stair, "Sources as radiometric standards," Adv. Geophys. **14**, 83-109 (1970).
[18]J. R. Hickey, "Laboratory methods of experimental radiometry including data analysis," Adv. Geophys. **14**, 227-267 (1970).
[19]P. B. Coates, "Tungsten ribbon lamps," in *Theory and Practice of Radiation Thermometry* (Wiley, New York, 1988), pp. 773–819.
[20]J. Roth, J. Appl. Phys. **35**, 1429 (1964).
[21]O. V. Fat'yanov, T. Ogura, M. F. Nicol, and K. Kondo, Infrared Phys. Technol. **42**, 55 (2001).
[22]I. M. Voskoboinikov and A. Ya. Apin, Sov. Phys.-Dokl. **130**, 804 (1960) (in Russian).
[23]G. Dunham, J. E. Bailey, A. Carlson, P. Lake, and M. D. Knudson, Rev. Sci. Instrum. **75**, 928 (2004); J. E. Bailey, M. D. Knudson, A. L. Carlson, G. S. Dunham, M. P. Desjarlais, D. L. Hanson, and J. R. Asay, Phys. Rev. B **78**, 144107 (2008).
[24]S. B. Kormer, K. B. Yushko, and G. V. Krishkevich, JETP Lett. **3**, 39 (1966) [ZhETF Pis. Red. **3**, 64 (1966)]; Sov. Phys. JETP **25**, 980 (1967) [J. Exptl. Theoret. Phys. (U.S.S.R.) **52**, 1478 (1967)].
[25]D. G. Hicks, T. R. Boehly, J. H. Eggert, J. E. Miller, P. M. Celliers, and G. W. Collins, Phys. Rev. Lett. **97**, 025502 (2006).
[26]R. G. Kraus, S. T. Stewart, D. C. Swift, C. A. Bolme, R. F. Smith, S. Hamel, B. D. Hammel, D. K. Spaulding, D. G. Hicks, J. H. Eggert, and G. W. Collins, J. Geophys. Res. **117**, E09009, doi:10.1029/2012JE004082 (2012).
[27]J. E. Miller, T. R. Boehly, A. Melchior, D. D. Meyerhofer, P. M. Celliers, J. H. Eggert, D. G. Hicks, C. M. Sorce, J. A. Oertel, and P. M. Emmel, Rev. Sci. Instrum. **78**, 034903 (2007).
[28]D. K. Spaulding, D. G. Hicks, R. F. Smith, J. H. Eggert, R. S. McWilliams, G. W. Collins, and R. Jeanloz, AIP Conf. Proc. **955**, 1071–1074 (2007).
[29]T. Kobayashi, T. Sekine, O. V. Fat'yanov, E. Takazawa, and Q. Y. Zhu, J. Appl. Phys. **83**, 1711 (1998).
[30]O. V. Fat'yanov, P. D. Asimow, and T. J. Ahrens, AIP Conf. Proc. **1195**, 855–858 (2009).
[31]J. Li, X. Zhou, J. Li, Q. Wu, L. Cai, and C. Dai, Rev. Sci. Instrum. **83**, 053902 (2012).
[32]M. B. Boslough, Ph.D. thesis, California Institute of Technology, Pasadena, 1984.
[33]B. Svendsen and T. J. Ahrens, Geophys. J. Int. **91**, 667 (1987).
[34]M. A. Barrios, D. G. Hicks, T. R. Boehly, D. E. Fratanduono, J. H. Eggert, P. M. Celliers, G. W. Collins, and D. D. Meyerhofer, Phys. Plasmas **17**, 056307 (2010).
[35]M. D. Johnston, B. V. Oliver, D. W. Droemer, B. Frogget, M. D. Crain, and Y. Maron, "Absolute calibration method for nanosecond-resolved, time-streaked, fiber optic light collection, spectroscopy systems," SANDIA Report No. SAND2010-2470, 2010.
[36]A. E. Voitenko, I. Sh. Model', and I. S. Samodelov, Sov. Phys.-Dokl. **11**, 596 (1967) [Dokl. Acad. Nauk SSSR **169**, 547 (1966)].
[37]F. E. Nicodemus, Am. J. Phys. **31**, 368 (1963).
[38]E. J. Gillham, "Radiometry from the viewpoint of the detector," Adv. Geophys. **14**, 53–81 (1970).
[39]W. Yang, Ph.D. thesis, California Institute of Technology, Pasadena, 1996.
[40]S. C. Gupta, S. G. Love, and T. J. Ahrens, Earth Planet. Sci. Lett. **201**, 1 (2002).
[41]Model 550 blackbody from Williamson Corporation, Concord, MA, U.S.A.; Model BBS 1500 blackbody calibration source from Process Sensors Corp. (Infrared Division), Franklin Lakes, NJ, U.S.A.
[42]A. J. Metzler and J. R. Branstetter, Rev. Sci. Instrum. **34**, 1216 (1963).
[43]K. C. Lapworth, T. J. Quinn, and L. A. Allnutt, "A black-body source of radiation covering a wavelength range from the ultraviolet to the infrared," J. Phys. E **3**, 116–120 (1970).
[44]S. M. Chernin, Appl. Opt. **36**, 1580 (1997), and references therein.
[45]D. B. Thomas, J. Res. Natl. Inst. Stand. Technol. **66C**, 255 (1962).
[46]B. B. Khlevnoi, S. A. Ogarev, V. I. Sapritskii, S. P. Morozova, M. L. Samoilov, M. K. Sakharov, V. B. Khromchenko, and V. I. Shapoval, Meas. Tech. **48**, 1083 (2005) [Izmer. Tekh. **48**, 29–34 (2005)].
[47]A. V. Murthy, B. K. Tsai, and R. D. Saunders, J. Res. Natl. Inst. Stand. Technol. **105**, 293 (2000).
[48]Graphite dual cavity blackbodies HT-5500 and HT-9500 from Thermo Gauge Instruments, Inc., Fort Ashby, WV, U.S.A.; Ultra high temperature blackbody calibrator Mikron M390 from LumaSense Technologies, Inc., Santa Clara, CA, U.S.A.
[49]G. W. Collins, P. M. Celliers, L. B. Da Silva, R. Cauble, D. M. Gold, M. E. Foord, N. C. Holmes, B. A. Hammel, R. J. Wallace, and A. Ng, Phys. Rev. Lett. **87**, 165504 (2001).

[50]A. Yu. Dolgoborodov, M. A. Brajnikov, M. N. Makhov, N. E. Safronov, and V. G. Kirilenko, Combust., Explos., Shock Waves **49**, 723–730 (2013) [Fiz. Goreniya Vzryva **49**, 112–120 (2013)].
[51]V. E. Bespalov, V. K. Gryaznov, A. N. Dremin, and V. E. Fortov, Sov. Phys. JETP **42**, 1046 (1975) [J. Exptl. Theoret. Phys. (U.S.S.R.) **69**, 2059 (1975)].
[52]Yu. A. Zatsepin, E. G. Popov, and M. A. Tsikulin, Sov. Phys. JETP **27**, 63 (1968) [J. Exptl. Theoret. Phys. (U.S.S.R.) **54**, 112 (1968)].
[53]V. G. Ageev, A. V. Bushman, M. I. Kulish, M. E. Lebdev, A. A. Leont'ev, V, Ya. Ternovoi, A. S. Filimonov, and V. E. Fortov, JETP Lett. **48**, 659 (1988) [ZhETF Pis. Red. **48**, 608 (1988)].
[54]H. B. Radousky, M. Ross, A. C. Mitchell, and W. J. Nellis, Phys. Rev. B **31**, 1457 (1985).
[55]A. E. Voitenko, F. O. Kuznetsov, and I. Sh. Model', Instrum. Exp. Tech. **6**, 1184 (1962) [Prib. Tekh. Eksp. **6**, 121 (1962)].
[56]D. H. Dolan, Ph.D. thesis, Washington State University, Pullman, 2003, pp. 61, 110, 111, and 291.
[57]Light pulses from the SI-IMS300 Industrial Spectroscopy Flash Lamp (Specialized Imaging, Ltd., UK) recorded with the Caltech 6-channel shock-temperature pyrometer.
[58]S. Horne, D. Smith, M. Besen, M. Partlow, D. Stolyarov, H. Zhu, and W. Holber, Proc. SPIE **7680**, 76800L (2010); see also http://www.energetiq.com/DataSheets/LDLS_Selection_Guide.pdf.
[59]D. H. Dolan, C. T. Seagle, and T. Ao, "Dynamic temperature measurements with embedded optical sensors," SANDIA Report No. SAND2013-8203, 2013.
[60]C. R. Barber, J. Sci. Instrum. **23**, 238 (1946).
[61]R. Stair, R. G. Johnson, and E. W. Halback, J. Res. NBS **64A**, 291 (1960).
[62]H. J. Kostkowski, D. E. Erminy, and A. T. Hattenburg, "High-accuracy spectral radiance calibration of tungsten-strip lamps," Adv. Geophys. **14**, 111–127 (1970).
[63]W. E. Schneider and D. G. Goebel, Proc. SPIE **308**, 28 (1982).
[64]Tungsten ribbon lamps for the calibration of radiation thermometers, International recommendation IOLM R 48, International Organization of Legal Metrology, Paris, France, 2004.
[65]S. W. Brown, G. P. Eppeldauer, and K. R. Lykke, Appl. Opt. **45**, 8218 (2006).
[66]A. P. Levick, C. L. Greenwell, J. Ireland, E. R. Woolliams, T. M. Goodman, A. Bialek, and N. P. Fox, Appl. Opt. **53**, 3508 (2014).
[67]C. E. Gibson, B. K. Tsai, and A. C. Parr, NIST MEASUREMENT SERVICES: Radiance Temperature Calibrations, NIST Special Publication 250-43, Gaithersburg, Maryland, U.S.A. 1998; see also http://www.nist.gov/calibrations/spectroradiometric.cfm.
[68]Model 550G from Optronic Laboratories, Inc., Orlando, FL, U.S.A. with 18A/T10/1 type lamp from General Electric, U.S.A. calibrated for use at 15.0 A.
[69]R. Stair, W. E. Schneider, and J. K. Jackson, Appl. Opt. **2**, 1151 (1963); R. Stair, W. E. Schneider, and W. B. Fussel, *ibid.* **6**, 101 (1967).
[70]M. Ojanen, P. Kärhä, S. Nevas, A. Sperling, H. Mäntynen, and E. Ikonen, Metrologia **49**, S53 (2012).
[71]N. C. Holmes, M. Ross, and W. J. Nellis, Phys. Rev. B **52**, 15835 (1995).
[72]L. K. Thomas, J. Appl. Phys. **39**, 4681 (1968).
[73]D. B. Keck, Appl. Opt. **13**, 1882 (1974).
[74]M. Imai and E. H. Hara, Appl. Opt. **13**, 1893 (1974).
[75]J. Dugas, M. Sotom, L. Martin, and J. M. Cariou, Appl. Opt. **26**, 4198 (1987).
[76]R. Payne and L. O. Bouthillette, Appl. Opt. **17**, 2132 (1978).
[77]F. T. Stone, Appl. Opt. **17**, 2825 (1978).
[78]M. Bart, E. W. M. van der Ham, and P. Saunders, Int. J. Thermophys. **28**, 2111 (2007); P. Saunders and H. Edgar, Metrologia **46**, 62 (2009).
[79]J. C. Solorio-Leyva, J. G. Suárez-Romero, J. G. Cortés-Reynoso, J. B. Hurtado-Ramos, and E. Tepichín-Rodríguez, Appl. Opt. **44**, 2511 (2005).
[80]H. W. Yoon, D. W. Allen, C. E. Gibson, M. Litorja, R. D. Saunders, S. W. Brown, G. P. Eppeldauer, and K. R. Lykke, Appl. Opt. **46**, 2870 (2007).
[81]R. Winkler, E. R. Woolliams, W. S. Hartree, S. G. R. Salim, N. P. Fox, J. R. Mountford, M. White, and S. R. Montgomery, Int. J. Thermophys. **28**, 2087 (2007).
[82]R. M. Pon and J. P. Hessler, Appl. Opt. **23**, 975 (1984), and references therein.
[83]Tektronix 4000 Series Digital Phosphor Oscilloscopes User Manual, p. 31 (Tektronix, Inc., Beaverton, Oregon, U.S.A.); available online at http://www.manualslib.com/manual/628846/Tektronix-4000-Series.html?page=49#manual or at http://122.physics.ucdavis.edu/course/cosmology/sites/default/files/files/Muon%20Lifetime/mso4000.pdf.
[84]G. Beck, Rev. Sci. Instrum. **47**, 537 (1976).
[85]J. A. Cline, C. D. Jonah, and D. M. Bartels, Rev. Sci. Instrum. **73**, 3908 (2002).
[86]G. A. Lyzenga, Ph.D. thesis, California Institute of Technology, Pasadena, 1980.
[87]S. B. Kormer, M. V. Sinitsyn, G. A. Kirillov, and L. T. Popova, Sov. Phys. JETP **22**, 97 (1966) [J. Exptl. Theoret. Phys. (U.S.S.R.) **49**, 135 (1965)].
[88]B. C. Reed, Am. J. Phys. **57**, 642 (1989). We used the correct expression for "overall" data point weight W_i in the form of $W_i = W(x_i)W(y_i)/[m^2W(x_i) + W(y_i)]$ instead of incorrectly published there $W_i = W(x_i)W(y_i)/[m^2W(y_i) + W(x_i)]$ (Equation (8) of Ref. 88).
[89]Ch. Santschi and M. J. Rossi, Phys. Chem. Chem. Phys. **6**, 3447 (2004).
[90]D. A. Patterson, Phys. Rev. **127**, 1564 (1962).
[91]M. S. Vassiliou and T. J. Ahrens, Geophys. Res. Lett. **8**, 729, doi:10.1029/GL008i007p00729 (1981).